# Modeling and Optimization the Influence of $CO_2$-MAG Welding Parameters on the Weld Joint Shape Factors

**Dr. Samir Ali Amin Alrabii**
Assistant Professor
Department of Mechanical Engineering
University of Technology
(alrabiee2002@yahoo.com)

**TarekM. A. Al**
Assistant Lecturer
Department of Applied Sciences
University of Technology
(tarekza@yahoo.com)

## ABSTRACT

This paper represents an experimentalattempt to predict the influence of CO2-MAG welding variables on the shape factors of the weld joint geometry. Theinput variables were welding arc voltage, wire feeding speed and gas flow rate to investigate their effects on the shape factorsof the weld joint geometry in terms of weld joint dimensions (bead width, reinforcement height, and penetration). Design of experiment with response surface methodology technique was employed to buildmathematical models for shape factors in terms of the input welding variables. Thepredicted models were found quadratic type and statistically checked by ANOVA analysis for adequacy purpose. Also, numerical and graphical optimizations were carried out to determine the optimum values for all responses and input variables. The optimum values of the voltage, wire feeding speed, gas flow rate, WPSF, and WRFF are (20 Volt), (153 cm/min), (10 L/min), (5.222), and (3.970), respectively. And, a good agreement was found between the experimental and predicted results. The weld joint efficiency was found (73%) at the optimum conditions.

**Keywords**:bead dimensions, WPSF, WRFF, CO2-MAG welding, joint efficiency.

## نمذجة وامثلية تأثير متغيرات لحام القوس المعدني بغاز $CO_2$ على عوامل شكل وصلة اللحام

**د. سمير علي أمين الربيعي**
أستاذ مساعد
قسم الهندسة الميكانيكية
الجامعة التكنولوجية

**طارق محمد علي علي**
مدرس مساعد
قسم العلوم التطبيقية
الجامعة التكنولوجية

**الخلاصة**

يمثل هذا البحث محاولة عملية لتنبأ تأثير متغيرات لحام القوس المعدني بغاز ($CO_2$) على عوامل الشكل الهندسي لوصلة اللحام. المتغيرات الداخلة هي طاقة القوس وسرعة تغذية سلك اللحام ومعدل جريان الغاز لبحث تأثيراتها على عوامل الشكل الهندسي لوصلة اللحامبدلالة أبعاد وصلة اللحام (عرض درزة اللحام وارتفاع التقوية والنفاذية) . تم تطبيق تقنية تصميم التجارب مع طريقة الاستجابة السطحية لبناء نماذج رياضية لعوامل الشكل بدلالة متغيرات اللحام الداخلة. وجدت نماذج التنبوء بالنوع التربيعي ودققت أحصائيا" بتحليل التباين (ANOVA) لغرض الملائمة. أجريت أيضا" الامثلية العددية والبيانية لآيجاد القيم المثلى لجميع الاستجابات والمتغيرات الداخلة. والقييم المثلى هي (20) فولت ، (153) سم / دقيقة سرعة تغذية السلك ، (10) لتر / دقيقة معدل جريان الغاز ، (5.222) معامل شكل نفاذية اللحام و (3.970) معامل شكل تقوية اللحام. ووجد توافق جيد بين النتائج العملية والنظرية. ووجدت كفاءة وصلة اللحام (73%) عند الظروف المثلى..

## 1. INTRODUCTION

MAG stands for metal-active-gas arc welding. This is a variation of MIG welding, in which identical equipment is used, but the inert gas is replaced by carbon dioxide, which is chemically active, **Patel, and Patel, 2014**.CO2-MAG is a process in which the source of heat is an arc format between the consumable metal electrode and the work piece, and the arc and the molten puddle are protected from contamination by the atmosphere (i.e., oxygen and nitrogen) with an externally supplied gaseous shield of carbon dioxide or argon-carbon dioxide mixture. All the major commercial metals can be welded by this process, including carbon steels, low alloy and high alloy steels, stainless, aluminum, and copper titanium, zirconium and nickel alloys, **Jadeja, and Patel, 2013**. With CO2 shielding, the electrode tip is not heated directly by the arc plasma but by the arc heat conducted through the molten drop. The molten drop grows in size andfinally detaches by short circuiting or gravity, **Singla, et al., 2010**. During the investigation by **Boiko and Avisans, 2013**, it was revealed that different shielding gas gives different influence on the welding process, welding joint quality and also on the welding costs. CO2 shielding provides deeper penetration, **Reddy, 2012**.

In the automated applications, a precise means of selection of the process variables and control of weld bead shape has become essential, because the mechanical strength of weldis influenced not only by the composition of the metal, but also by the weld bead shape, **Hould, 1989**.Also, the weld pool geometry plays an important role in determining the mechanical and corrosion properties of the weld, **Dasgupta, and Mukherjee, 2013**. Also, optimization of the process variables to control and obtain the required shape and quality of weld joint is possible with these expressions. The quality of the weld joints depends on the bead geometry and shape factors. The weld joint is specified by the bead width, height of reinforcement, depth of penetration, weld reinforcement form factor (WRFF) and weld penetration shape factor (WPSF). **Figure 1** shows the transverse cross section of a weld bead geometry. WPSF and WRFF are also called as coefficients of internal shape and external shape, respectively. The ratio of bead width to penetration and bead width to reinforcement are termed as Weld Penetration Shape Factor and Weld Reinforcement Form Factor, respectively.

Nowadays, DOE has been more widely used in quality control, manufacturing, and system engineering disciplines for design or development of a new product and redesign of an existing product **DeVor et al., 1992**. Due to the highly competitive global industry, companies need to understand the impact of both operational and environmental variables and their interactions on system or product performance. Therefore, mathematical model–based optimization employing DOE is a powerful design technique for use by system analysts, engineers, and designers. Compared to many methods, DOE is a more efficient method among optimization models in terms of number of required experiments. Its applications and computations are also more time efficient **Antony, 2003**. Normally the use of DOE technique is combined with RSM and ANOVA statistical tests. In the present work, DOE software version 8 was used. The most popular designs within RSM designs are the central composite design (CCD) and Box-Behnken design. In the present work, the central composite design (CCD) was used in the RSM technique (**Benyounis, and Olabi, 2005**).

Many researchers have been previously carried out by using CO2-MAG welding processes considering mainly the effect of process variables on the structure and mechanical properties. In addition, most studies have attempted to model the directed measured bead width, bead height and bead penetration only, regardless of the important shape relations of the weld bead. But, some important shape relations, such as weld reinforcement form factor (WRFF) and weld penetration shape factor (WPSF) have significant impact on the quality of weld. However, there is few works (**Gunaraj and Murugan, 1999; Kumar, 2011**) have focused on studying the influence of process variables on WPSF and WRSF using the Design of Experiment (DOE) and Response Surface Methodology (RSM) technique for predicting, modeling and optimization purposes for CO2-MAG welding.

Therefore, the aim of this paper is to investigate experimentally the effect of input welding variables of CO2-MAG welding process (arc voltage, wire feeding speed and gas flow rate) on the weld joint shape factors (WPSF and WRFF) obtained by the measurements of bead width, height of reinforcement and depth of penetration through experiments based on the DOE design matrix. The analysis of variance (ANOVA) technique was adopted to check the level and degree of the direct or interactive effect of the input variables on these factors. RSM was applied to derive mathematical models, and the predicted equations were used to represent graphically the effects of process variables on the shape factor responses. No much work so far has been performed which considers the three process variables used in this study using DOE and RSM approach.

## 2. EXPERIMENTAL PROCEDURE

### 2.1 Material Verification

Low carbon steel material type AISI 1010 in form of plate with 5 mm thickness in the hot rolled condition was used in this work to prepare specimens for welding tests. The chemical analysis for this material was carried out, and the results are presented in Table 1. Also, three samples from this material were then prepared for tensile tests according to ASTM-E8 standard. The mechanical properties of this steel were obtained and the resulted data are given in Table 2, showing the average of three readings for three tested samples**.** These tables verify that the used material is in conformity with the standard base metal, **ASM, 1992**.

### 5.2 Specimens Preparation for Welding Tests

Specimens were then prepared from low carbon steel material type AISI 1010 with dimensions of 50 mm× 25 mm×5 mm to be welded in a closed butt weld joint design by CO2-MAG process. These specimens were then cleaned by a wire brush to remove the oxide layers and any surface defects.

### 2.3 Welding Variables

The effective selected input factors of CO2- MAG welding in this work were welding speed, arc voltage and wire feeding speed in two levels, as shown in Table 3. These parameters were used based on the ability of welding machine and experimental skill of the welder operator.

### 2.4 Welding Procedure

The machine employed for welding experimentation was 'INVERTER CO2 MAG - BEAM-350' in Korean-Iraqi Vocational Training Center in Baghdad. The welding wire type 'AWS ER70S-6'1.2 mm diameter in form of rod was used for welding specimens. $CO_2$-MAG welding tests were conducted for twenty samples using the welding factors mentioned above and depending on the design matrix established by Design of Experiment software, as given in Table 4.These tests were conducted randomly according the design matrix made by DOE program to prevent any systematic error.

### 2.5 Measurements of Weld Joint Dimensions and Shape Factors Calculations

After welding, transverse sections of the weld joints were cut from the middle portions of specimens. The specimens were prepared by grinding and polishing methods. The properly polished specimens were etched with a 2% Nital solution for about 30 seconds for measurements purpose. For each sectioned specimen, the important dimensions of the weld joints were measured by using a digital caliper. The average measurements of bead width, reinforcement height and depth of penetration were recorded to calculate the average weld penetration shape factor (WPSF) and average weld reinforcement form factor (WRFF) using the following equations, **Bahrami, et al., 2010**:

$$WPSF = \frac{W}{P} \quad (1)$$

Where, W = Width of the bead (mm).
P= Depth of penetration (mm).

$$WRFF = \frac{W}{R} \quad (2)$$

Where, R = Height of reinforcement (mm).

The results of calculations of shape factors as responses together with the input welding variables are listed in Table 4. With the help of these calculated responses, models were developed.

## 3. RESULTS AND DISCUSSION

The response surface methodology was employed using the Design of Expert software 'version 8' to determine the following predicted models for the shape factors of the weld joint geometry in terms of arc voltage, wire feeding speed and gas flow rate:

### 3.1 Mathematical Model of Weld Penetration Shape Factor (WPSF)

For the weld penetration shape factor (WPSF), the analysis of variance (ANOVA) was established by DOE software version 8, as shown in Table 5, illustrating that the input parameters individually (A and B), the interaction of wire feeding speed and gas flow rate (BC) and the quadratic terms of voltage ($A^2$) and wire feeding speed ($B^2$) are all statistically significant and have the greatest influence on the weld penetration shape factor response (WPSF) according to

their P-values (< 0.05). This table also depicts that the gas flow rate (C) has no significant effect on WPSF, since its P-value (>0.05).The lack of fit test indicates a good model, since it is insignificant with P-value greater than 0.05. So, this analysis indicates that this model is significant at 95% confidence. In addition, this model showed a good agreement between the predicted and actual values for weld penetration shape factor WPSF, as shown in **Fig.2**. Therefore, the final predicted equation for the WPSF in terms of the coded input factors is:

$$WPSF = +5.03 + 0.68 * A + 0.20 * B - 0.063 * C + 0.83 * B * C - 0.23 * A^2 - 0.33 * B^2 \quad (3)$$

And, the final equation in terms of actual factors is:

$$WPSF = -86.99497 + 9.74713 * Voltage - 8.34643E\text{-}004 * Wire\ feeding\ speed - 2.51597 * Gas\ flow\ rate + 0.016563 * Wire\ feeding\ speed * Gas\ flow\ rate - 0.22678 * Voltage^2 - 5.22843E\text{-}004 * Wire\ feeding\ speed^2 \quad (4)$$

**Figure 3** shows the interaction effect of wire feeding speed and gas flow rate on WPSF at 20 v voltage. It is evident from this figure that WPSF increases for all values of wire feeding speed, while it decreases with increasing gas flow rate. This is due to fact that WPSF= W/P, where W increases with increase of wire feeding speed, whereas P decreases with increasing gas flow rate. Thus, wire feeding speed has a positive effect on WPSF, while gas flow rate has a negative effect on WPSF.

The statistical properties of this model were diagnosed, and it was found that the residuals that falling on a straight line implying errors are normally distributed, as shown in **Fig.4**. Additionally, the residuals versus predicted actual for WPSF data revealed no obvious pattern or unusual structure, as shown in **Fig.5**.

The perturbation of the predicted WPSF response resulted by varying only one parameter at a time from the center point of the investigated region is shown in **Fig.6**. It can be seen that increasing the voltage and wire feeding speed generally increases the WPSF, since these input parameters increased the fusion effect of the weld joint, which resulted in the increase of bead width. While, the gas flow rate had a very little effect on WPSF.

Due to no statistical problems found, the response surface plot was generated in terms of 2D surface plot as shown in **Figs.7**, depicting WPSF as a function of voltage and wire feeding speed at various gas flow rate10 L/min. This figure indicates that both voltage and wire feeding speed have greater influence on increasing WPSF. This is possibly due to increase of molten material accumulated in the weld joint caused by higher voltage and wire feeding speed. Also, this is more likely ascribed to the increased chemical reaction of $CO_2$ with the accumulated molten material in the weld joint.

**Figures 8** shows the 3D surface plot for WPSF as a function of voltage and wire feeding speed at 10 L/min gas flow rate, showing the similar behavior as mentioned above; higher WPSF occurred at higher values of voltage and wire feeding speed.

### 3.2 Mathematical Model of Weld Reinforcement Form Factor (WRFF)

Similarly, the analysis of variance (ANOVA) for RSM reduced quadratic model was determined for the weld reinforcement form factor (WRFF) given in Table 6. The results in this table show

that the voltage (A), wire feeding speed (B) and their squared terms ($A^2$ and $B^2$ ) are statistically significant, since their P-values were very small (< 0.5).While, the gas flow rate term (C) has no influence on the weld joint, since it is not seen in this analysis (model).Moreover, this table also reveals that the lack of fit is insignificant (P-value > 0.05), indicating that this model is adequate and significant at 95% confidence. So, the final predicted equation for the WRFF in terms of the coded input factors is:

$$WRFF = + 3.90 + 0.12 * A + 0.68 * B - 0.55 * A^2 - 0.29 * B^2 \quad (5)$$

And, the final equation in terms of actual factors:

$$WRFF = - 231.85179 + 21.99545 * Voltage + 0.16738 * Wire\ feeding\ speed - 0.54684 * Voltage^2 - 4.67743E\text{-}004 * Wire\ feeding\ speed^2 \quad (6)$$

The adequacy of this model was checked to examine the predicted model. Two types of model diagnostics, the normal probability plot and the residuals versus the actual values plot, were used for verification, as shown in **Figs. 9 and 10** for WRFF, respectively. It can be observed from these plots that there was no violation of the normality assumption, since the normal probability plot followed a straight line pattern, the residual was normally distributed, and as long as the residuals versus the predicted values show no unusual pattern and no outliers. Also, this model shows a good agreement between the predicted and actual values for WRFF, as depicted in **Fig.11**. The perturbation plot of the predicted responses caused by changing only one factor at a time from the center point of the experimental region is shown in **Fig. 12.** This figure indicates that, individually, the wire feeding speed has greater effect than the voltage on WRFF, since WRFF first increased and then decreased with increasing the voltage. This is more probably because of increasing wire feeding speed resulted in an increase in the bead with, leading to more accumulation of molten material due to more thermal effect and less chemical affinity of the $CO_2$gas with the weld joint material. Also, the decrease of WRFF at higher values of voltage is more likely due to the increase of reinforcement height that resulted from less bead penetration depth.

Because of no statistical problem with the model, **Fig. 13**shows the 2D contour plot for WRFF as a function of voltage and wire feeding speed at gas flow rate of 10 L/min. This figure exhibits that WRFF increases with increasing both voltage and wire feeding speed up to (20 volt) due to their combined effect by increasing the bead width. Whereas, **Figs. 14** depicts the 3D surface plot for the WRFF at gas flow rate 10 L/min. It can be noted from this figure that increasing both voltage and wire feeding speed increases the WRFF due to the increase of quantity of the molten material that resulted by the increase of bead width and thermal effect.

### 3.3 NUMERICAL OPTIMIZATION

The numerical optimization is provided by the Design of Experiment software to find out the optimum combinations of parameters in order to fulfill the requirements as desired. Therefore, this software was used for optimizing WPSF and WRFF; based on the data from the predicted models as a function of three factors: arc voltage, wire feeding speed and gas flow rate.

Table 7 shows constrains of each variable for numerical optimization of the WPSF and WRFF. According to this table, one possible run fulfilled the specified constrains to obtain the optimum

values for WPSF and WRFF and desirability, as listed in Table 8. It can be noted that this run gave a desirability of 0.849 with the optimum values of the voltage (20 volt), wire feeding speed (153 cm/min), and gas flow rate (10 L/min). **Figures 15-17** manifest the 3D surface plots for desirability, optimum value of WPSF (5.222)and optimum value of WRFF (3.970), respectively as a function of voltage and wire feeding speed at 10 L/min gas flow rate.

### 3.4. GRAPHICAL OPTIMIZATION

**Figure 18** depicts the overlay plot produced by the graphical optimization in DOE. In this figure, the regions not meeting the required variables are shaded out, leaving an operating window or "sweet spot". This means that the shaded area on the graphical optimization plot do not meet the selection criteria, and the clear 'window' shows where one can set the variables to satisfy the requirements for both responses. The flag is planted at the optimum values of welding variables and responses.

### 3.5. EFFICIENCY OF THE WELD JOINT

In order to obtain the efficiency of the weld joint obtained by $CO_2$-MAG welding of low carbon steel AISI 1010, three tensile samples were first welded with the optimum welding condition given in Table 8 and then tensile tested to determine the ultimate tensile strength of the weld joint. The average tensile strength was found to be 285 MPa. Therefore, the efficiency of the weld joint was calculated to be 73% according to the joint efficiency definition which is the ratio of the tensile strength of the weld joint to the tensile strength of the base metal (Table 2). This result indicates the importance of using $CO_2$-MAG welding process and its effectiveness and suitability for welding steel AISI 1010 from strength point of view.

## 4. CONCLUSIONS

1. Regarding the WPSF, a quadratic model was obtained by DOE with RSM technique for the optimum WPSF response in terms of input welding parameters. This model indicated that the arc voltage and wire feeding speed are largely effective on WPSF, while the gas flow rate is not influential.
2. The interaction effect in WPSF model indicated that the wire feeding speed has a positive influence on WPSF response, while the gas flow rate has a negative effect on WPSF.
3. Concerning the WRFF, a quadratic model was obtained for the optimum WRFF response in terms of input welding parameters. This model shows that the wire feeding speed has greater impact than voltage on WRFF, whereas the gas flow rate was found not effective.
4. By numerical optimization, the optimum values of the voltage, wire feeding speed, gas flow rate, WPSF,WRFF and desirability are (20 Volt), (153 cm/min), (10 L/min), (5.222), (3.970) and (0.849), respectively.
5. The overlay plot produced by the graphical optimization is very useful to show the window of operability, where the requirements simultaneously meet the critical properties.
6. Using $CO_2$-MAG welding process is importantly effective and suitable for welding steel AISI 1010 from the strength point of view (with 73% joint efficiency).
7. DOE with RSM was found a useful tool for predicting the responses in MAG-$CO_2$ welding technique for any given input parameters.

## REFERENCES


- Antony, J., 2003, *Design of Experiments for Engineers and Scientists* ISBN: 0750647094, Elsevier Science and Technology Books.
- ASM Materials Engineering Dictionary,1992, Edited by Joseph R. Davis, *Table 13 on Page 13*, ASM International.
- Benyounis, K. Y., and Olabi, A. G., 2005, *Effect of Laser-Welding Parameters on the Heat input and Weld-Bead Profile*, Journal of Materials Processing Technology, Vol. 164-165, PP. 978-985.
- Boiko, I., and Avisans, D., 2013, *Study of Shielding Gases for MAG*, Materials Physics and Mechanics, 16, PP. 126-134.
- Dasgupta, E. B., and Mukherjee, S., 2013, *Optimization of Weld Bead Parameters of Nickel Based Overlay Deposited By Plasma Transferred Arc Surfacing*, International Journal of Modern Engineering Research (IJMER), Vol.3, Issue.3, PP. 1330-1335.
- DeVor, R. E., Chang, T–h., and Sutherland, J. W., 1992, *Statistical Quality Design and Control — Contemporary Concepts and Methods*, New Jersey: Prentice–Hall, Inc., PP. 542–562.
- Gunaraj,V., and Murugan, N., 1999, *Application of Response Surface Methodology for Predicting Weld Bead Quality in SAW of pipes*, Journal of Materials Processing Technology, Vol. 88, PP. 266-275.
- Hould, C. P. T., 1989, *Submerged Arc Welding*, Second Edition, Abington Publishing, Cambridge, England.
- Jadeja D. V., and Patel, S. P., 2013, *A Review on Parametric Optimization by Factorial Design Approach of Mag-$CO_2$ Welding Process*, International Journal of Engineering Research and Applications (IJERA), Vol. 3, Issue 2, PP. 420-424.
- Kumar, V., 2011, *Modeling of Weld Bead Geometry and Shape Relationships in Submerged Arc Welding using Developed Fluxes*, Jordan Journal of Mechanical and Industrial Engineering, Vol. 5, No. 5, PP. 461-470.
- Patel, P. D., and Patel, S. P., 2014, *Prediction of Weld Strength of Metal Active Gas (MAG) Welding Using Artificial Neural Network*, International Journal of Engineering Research and Applications (IJERA), Vol. 1, Issue 1, PP. 036-044.
- Reddy, A. C., 2012, *Studies on the Effects of Oxidation and Its Repression in MAG Welding Process*, International Journal of Advanced Research in Engineering and Technology (IJARET), Vol. 3, No.1, PP. 48-54.
- Singla M., Singh, D., and Deepak, D., 2010, *Parametric Optimization of Gas Metal Arc Welding Processes by Using Factorial Design Approach*, Journal of Minerals and Materials Characterization and Engineering, Vol. 9, No.4, PP. 353-363.
- **www.efunda.com**, *Mechanical Properties of steel AISI 1010*.

**Table 1.** Chemical Composition for used LCS with standard type (wt%).

| Material | C | Si | Mn | P | S | Cr | Mo | Ni | V | Fe |
|---|---|---|---|---|---|---|---|---|---|---|
| Experimental | 0.13 | 0.01 | 0.450 | 0.003 | 0.003 | 0.001 | 0.002 | 0.043 | 0.001 | Bal. |
| Standard Steel AISI 1010 [ASM, 1992] | 0.08 – 0.13 | 0.1 max | 0.3 - 0.6 | 0.04 max | 0.05 max | -- | -- | -- | -- | Bal. |

**Table 2.** Mechanical properties for used LCS with standard type

| Material | Yield strength (MPa) | Tensile strength (MPa) | Reduction in Area (%) |
|---|---|---|---|
| Experimental | 262 | 391 | 42 |
| Standard steel 1010 [www.efunda.com] | 305 | 365 | 40 |

**Table 3.** Levels of input parameters used with respective coding.

| Input parameter | Unit | Low Level - 1 | High Level + 1 | -alpha | +alpha |
|---|---|---|---|---|---|
| Voltage | volt | 19 | 21 | 18 | 22 |
| Wire feeding speed | cm/min | 125 | 175 | 100 | 200 |
| Gas flow rate | L/min | 8 | 12 | 5 | 14 |

**Table 4.** Design matrix for input factors and experimental values of output (responses)

| Std | Run No. | Type of point | Voltage (volt) | Wire feeding speed (cm/min) | Gas flow rate (L/min) | WPSF | WRFF |
|---|---|---|---|---|---|---|---|
| 1 | 12 | Factorial | 19 | 125 | 8 | 4.404 | 2.530 |
| 2 | 7 | Factorial | 21 | 125 | 8 | 5.921 | 2.500 |
| 3 | 8 | Factorial | 19 | 175 | 8 | 3.100 | 3.500 |
| 4 | 1 | Factorial | 21 | 175 | 8 | 4.600 | 3.800 |
| 5 | 14 | Factorial | 19 | 125 | 12 | 2.900 | 2.200 |
| 6 | 4 | Factorial | 21 | 125 | 12 | 3.900 | 2.400 |
| 7 | 16 | Factorial | 19 | 175 | 12 | 4.700 | 3.600 |
| 8 | 18 | Factorial | 21 | 175 | 12 | 6.100 | 3.900 |
| 9 | 9 | Axial | 18 | 150 | 10 | 2.800 | 1.500 |
| 10 | 15 | Axial | 22 | 150 | 10 | 5.500 | 2.000 |
| 11 | 6 | Axial | 20 | 100 | 10 | 3.300 | 1.400 |
| 12 | 2 | Axial | 20 | 200 | 10 | 4.200 | 4.136 |
| 13 | 19 | Axial | 20 | 150 | 6 | 5.293 | 4.000 |
| 14 | 10 | Axial | 20 | 150 | 14 | 5.000 | 4.050 |
| 15 | 3 | Center | 20 | 150 | 10 | 5.300 | 4.050 |
| 16 | 11 | Center | 20 | 150 | 10 | 4.963 | 3.800 |
| 17 | 17 | Center | 20 | 150 | 10 | 5.200 | 3.715 |
| 18 | 5 | Center | 20 | 150 | 10 | 5.100 | 3.900 |
| 19 | 13 | Center | 20 | 150 | 10 | 4.700 | 4.100 |
| 20 | 20 | Center | 20 | 150 | 10 | 4.800 | 3.750 |

**Table 5.** Analysis of variance (ANOVA) for response surface reduced quadratic model (WPSF).

| Source | Sum of squares | df | Mean square | F value | p-value Prob > F |
|---|---|---|---|---|---|
| Model | 17.09 | 6 | 2.85 | 90.74 | < 0.0001 significant |
| A-Voltage | 7.31 | 1 | 7.31 | 233.05 | < 0.0001 |
| B-Wire feeding speed | 0.63 | 1 | 0.63 | 20.08 | 0.0006 |
| C-Gas flow rate | 0.064 | 1 | 0.064 | 2.04 | 0.1772 |
| BC | 5.49 | 1 | 5.49 | 174.84 | < 0.0001 |
| $A^2$ | 1.36 | 1 | 1.36 | 43.19 | < 0.0001 |
| $B^2$ | 2.81 | 1 | 2.81 | 89.68 | < 0.0001 |
| Residual | 0.41 | 13 | 0.031 | | |
| Lack of Fit | 0.14 | 8 | 0.017 | 0.32 | 0.9276 not significant |
| Purr Error | 0.27 | 5 | 0.054 | | |
| Core Total | 17.49 | 19 | | | |
| Std. Dev. = 0.18 | | | R-Squared = 0.9767 | | |
| Mean = 4.59 | | | Adj R-Squared = 0.9659 | | |
| C.V. % = 3.86 | | | Pred R-Squared = 0.9580 | | |
| PRESS = 0.73 | | | Adeq Precision = 32.493 | | |

**Table 6.** Analysis of variance (ANOVA) for response surface reduced quadratic model (WRFF)

| Source | Sum of squares | df | Mean square | F value | p-value Prob > F |
|---|---|---|---|---|---|
| Model | 16.48 | 4 | 4.12 | 295.50 | < 0.0001 significant |
| A-Voltage | 0.24 | 1 | 0.24 | 17.04 | 0.0009 |
| B-Wire feeding speed | 7.32 | 1 | 7.32 | 524.97 | < 0.0001 |
| $A^2$ | 7.88 | 1 | 7.88 | 565.18 | < 0.0001 |
| $B^2$ | 2.25 | 1 | 2.25 | 161.52 | < 0.0001 |
| Residual | 0.21 | 15 | 0.014 | | |
| Lack of Fit | 0.081 | 10 | 8.113E-003 | 0.32 | 0.9425 not significant |
| Purr Error | 0.13 | 5 | 0.026 | | |
| Core Total | 16.69 | 19 | | | |
| Std. Dev. = 0.12 | | | R-Squared = 0.9875 | | |
| Mean = 3.23 | | | Adj R-Squared = 0.9841 | | |
| C.V. % = 3.65 | | | Pred R-Squared = 0.9812 | | |
| PRESS = 0.31 | | | Adeq Precision = 45.824 | | |

**Table 7.** Constrains used for the numerical optimization.

| Name | Goal | Lower Limit | Upper Limit | Lower Weight | Upper Weight | Importance |
|---|---|---|---|---|---|---|
| A:Voltage | is in range | 19 | 21 | 1 | 1 | 3 |
| B:Wire feeding speed | is in range | 125 | 175 | 1 | 1 | 3 |
| C:Gas flow rate | is in range | 8 | 12 | 1 | 1 | 3 |
| Welding velocity | minimize | 64.66 | 125 | 1 | 1 | 3 |
| Arc energy | maximize | 230 | 1800 | 1 | 1 | 3 |
| WPSF | maximize | 2.8 | 6.1 | 1 | 1 | 3 |
| WRSF | maximize | 1.4 | 4.136 | 1 | 1 | 3 |

**Table 8.** Optimum solution of the desirability .

| Numer | Voltage | Wire feeding speed | Gas flow rate | WPSF | WRFF | Desirability |
|---|---|---|---|---|---|---|
| 1 | 20 | 153 | 10 | 5.222 | 3.970 | 0.849 Selected |

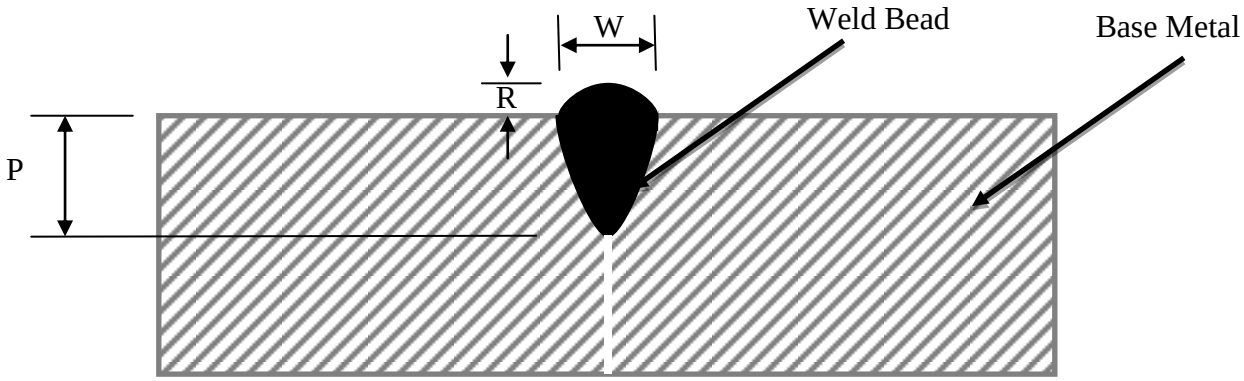


**Figure 1.** Weld bead geometry.

(P: Penetration, W: Bead Width, R: Bead Reinforcement)

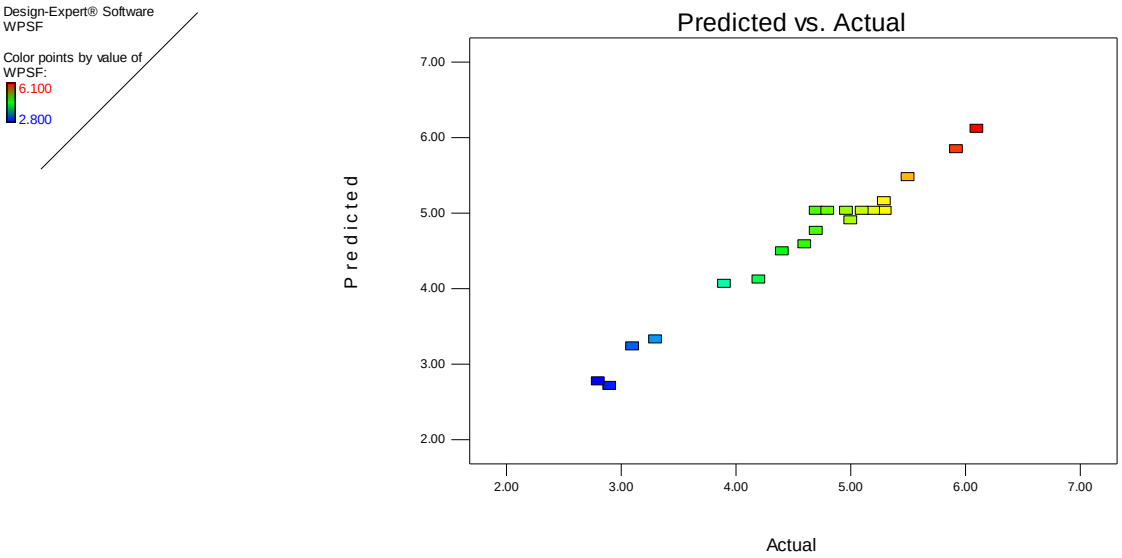


**Figure 2.** Predicted versus actual WPSF data.

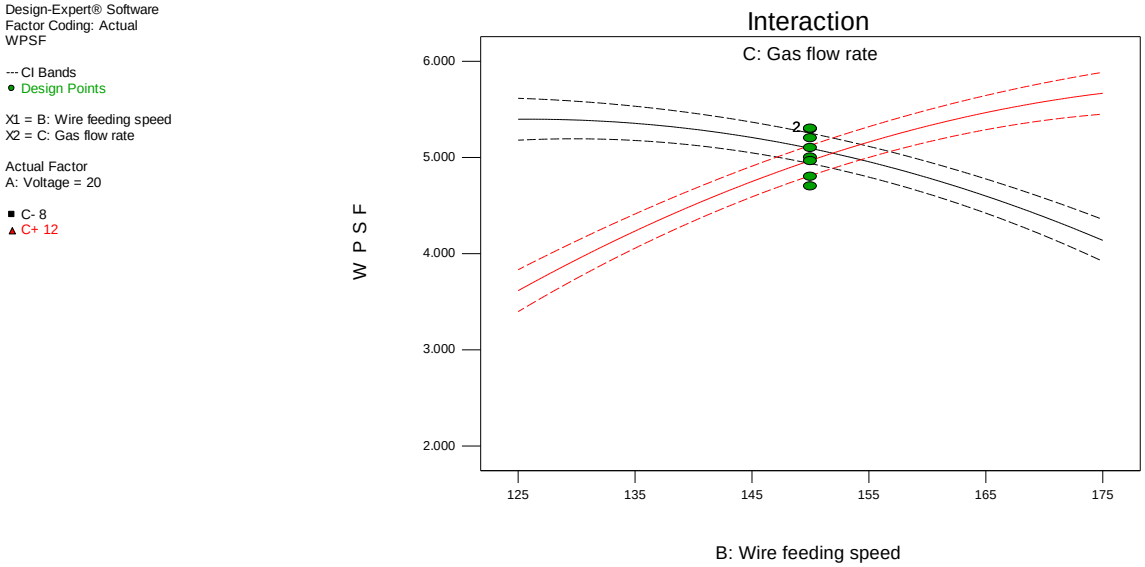


**Figure 3.** Effect of interaction of wire feeding speed and gas flow rate on WPSF.

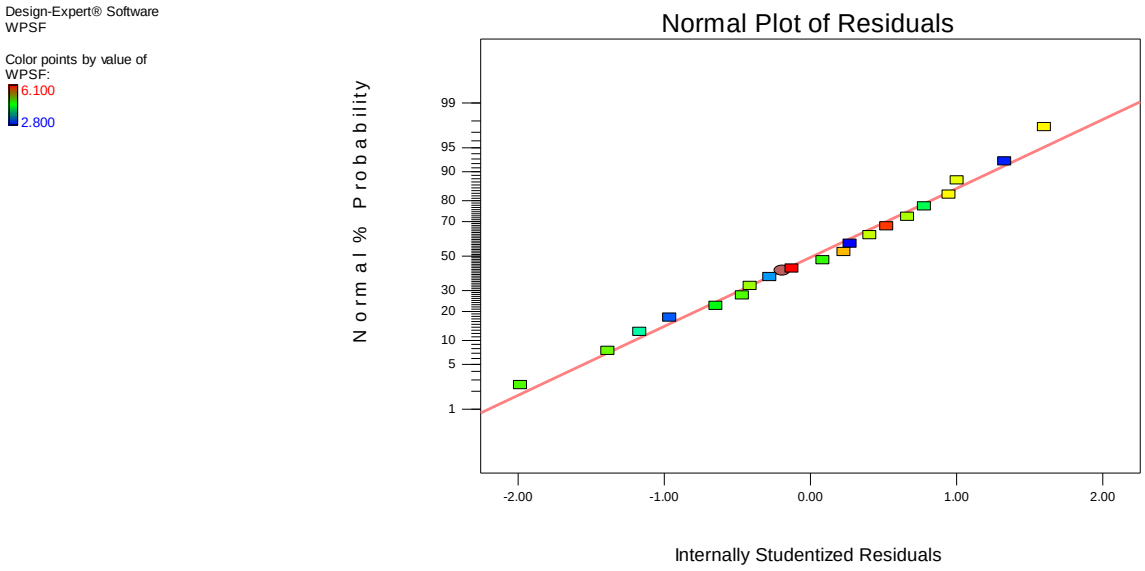


**Figure 4.** Normal probability plot of residuals for WPSF data.

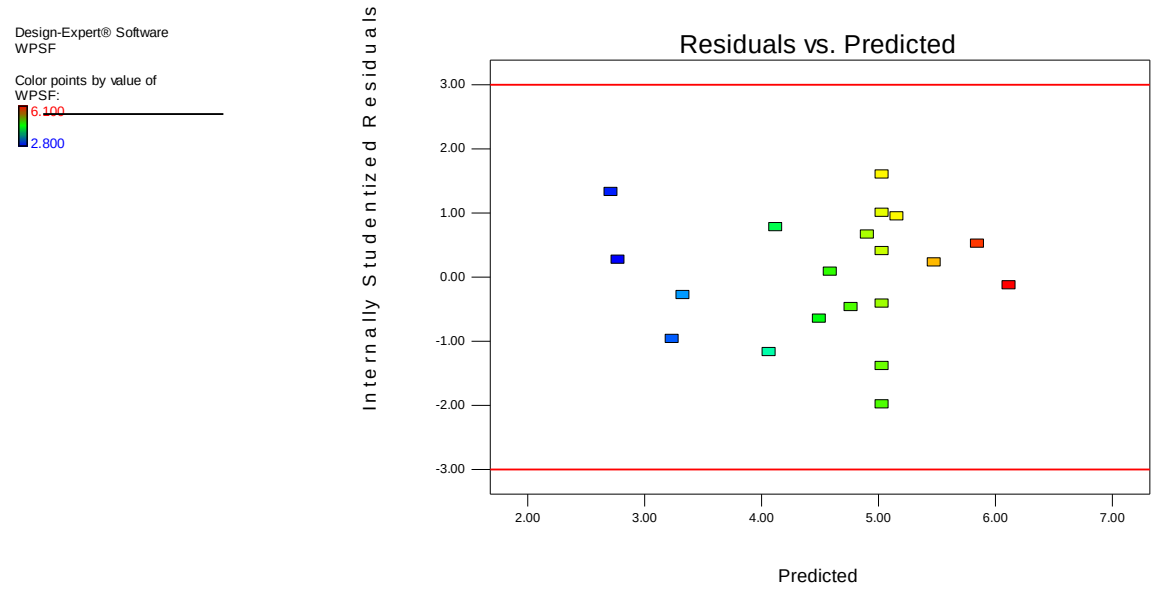


**Figure 5. Residuals versus predicted WPSF data.**

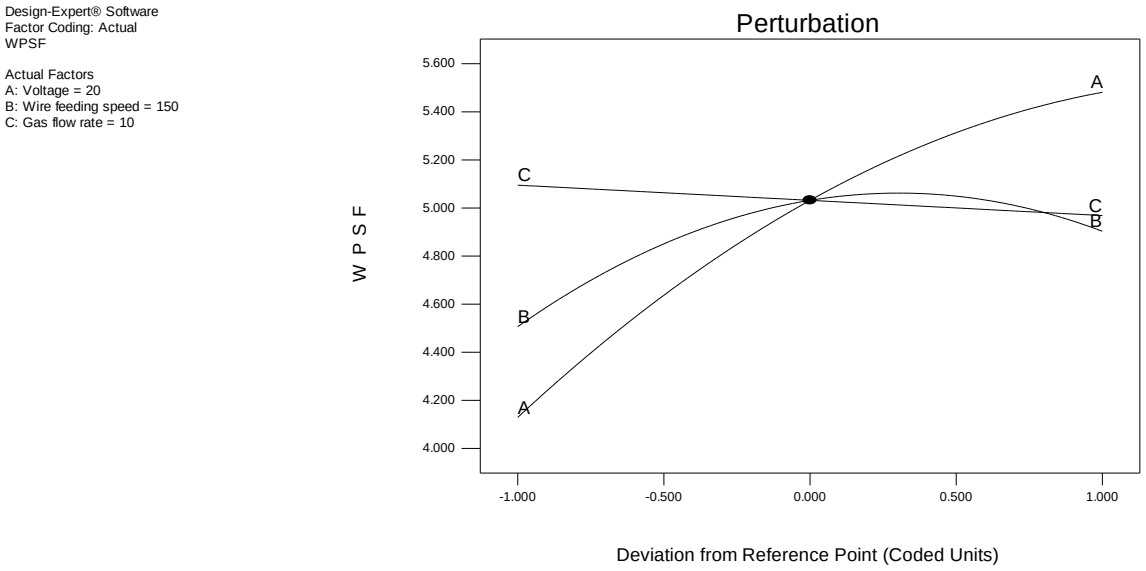


**Figure 6.** Perturbation of WPSF on wire feeding speed and gas flow rate.

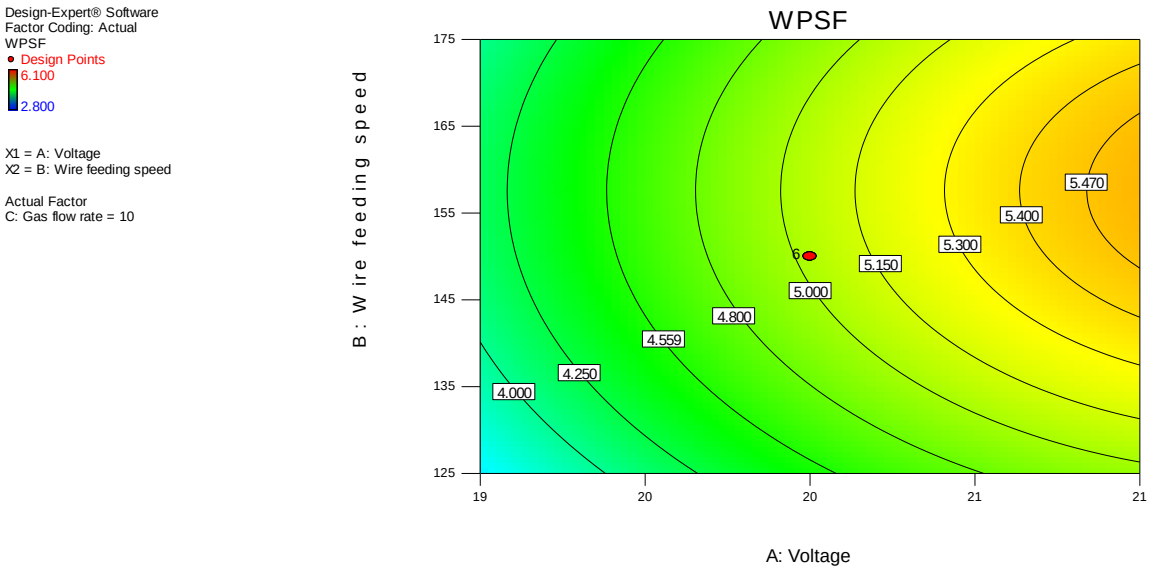


**Figure 7.** Contour graph WPSF as a function of voltage and wire feeding speed gas flow rate 10 L/min.

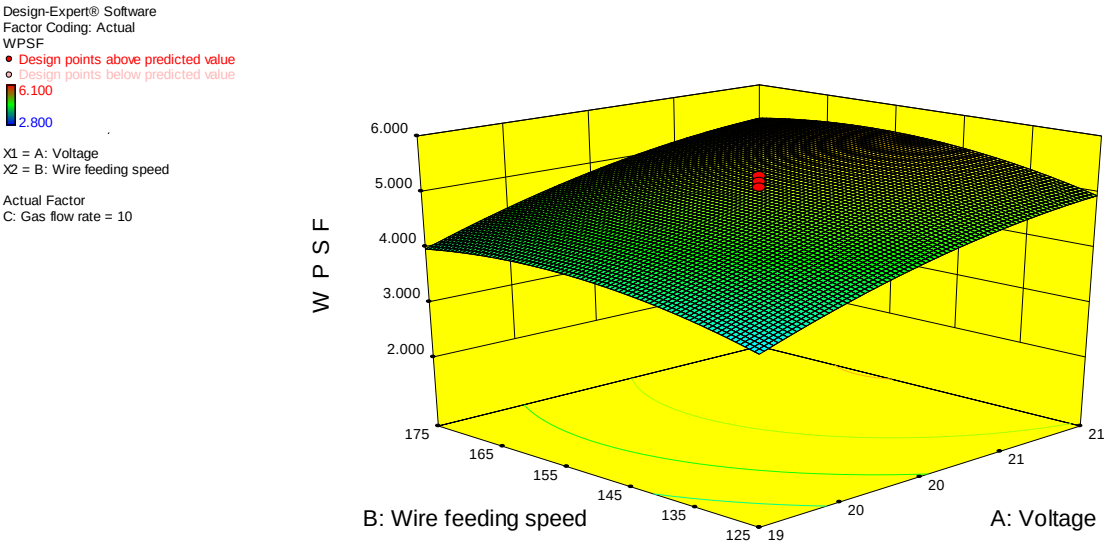


**Figure 8.** 3D graph of WPSF as a function of voltage and wire feeding speed at gas flow rate 10 L/min.

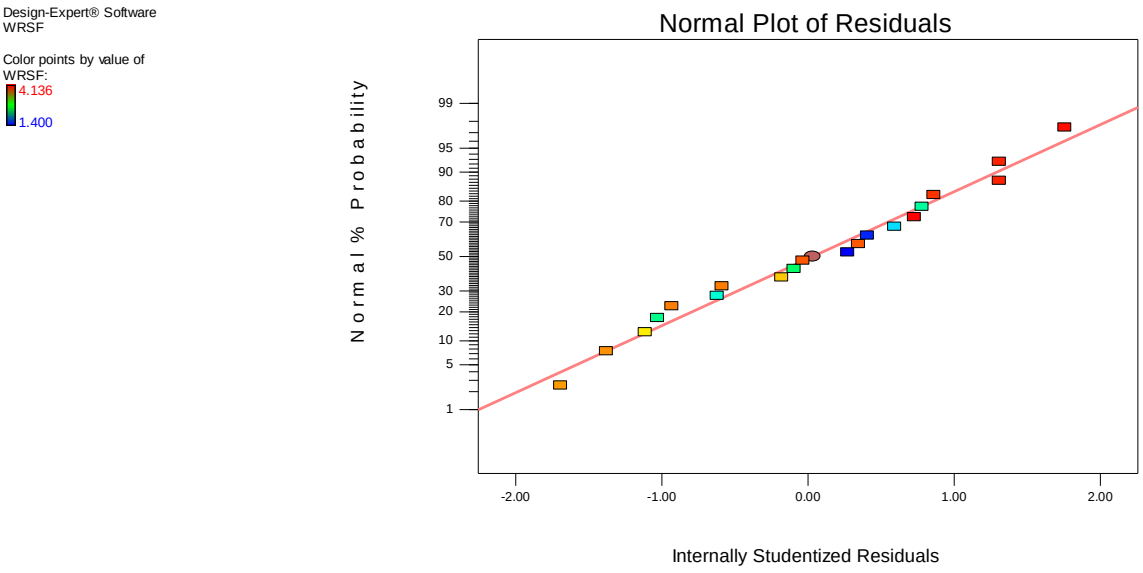


**Figure 9.** Normal probability plot of residuals for WRFF data.

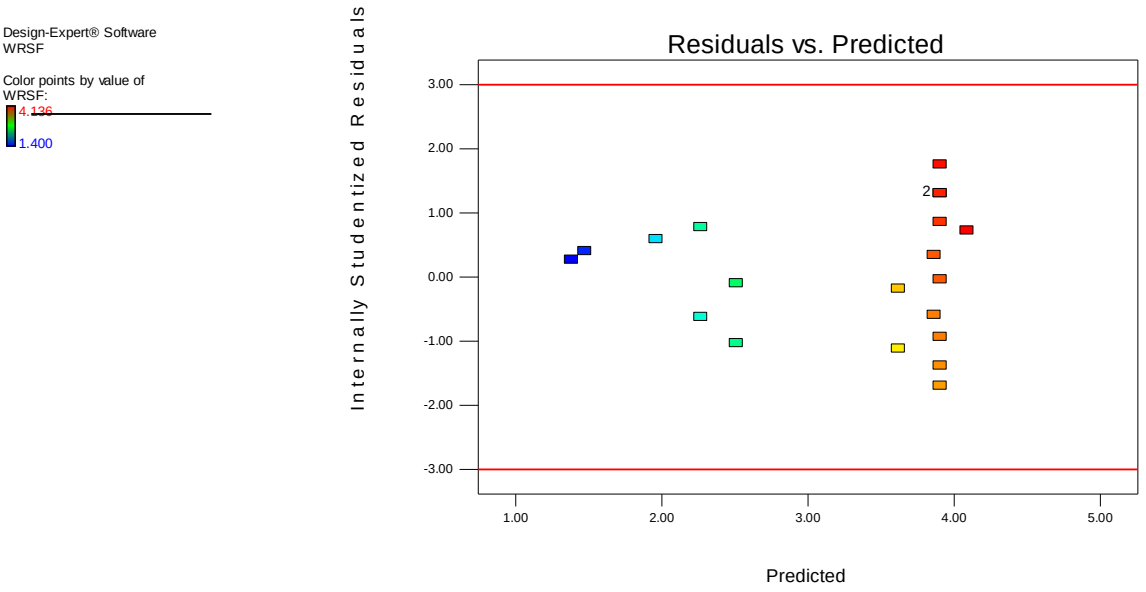


**Figure 10.** Residuals versus predicted WRFF data.

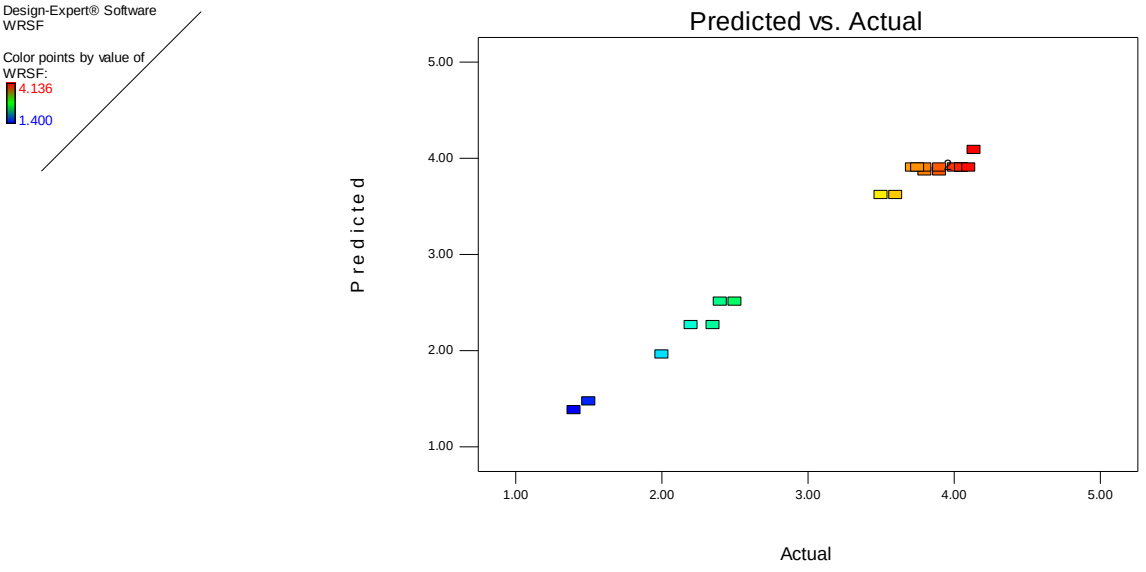


**Figure 11.** Predicted versus actual WRFF data.

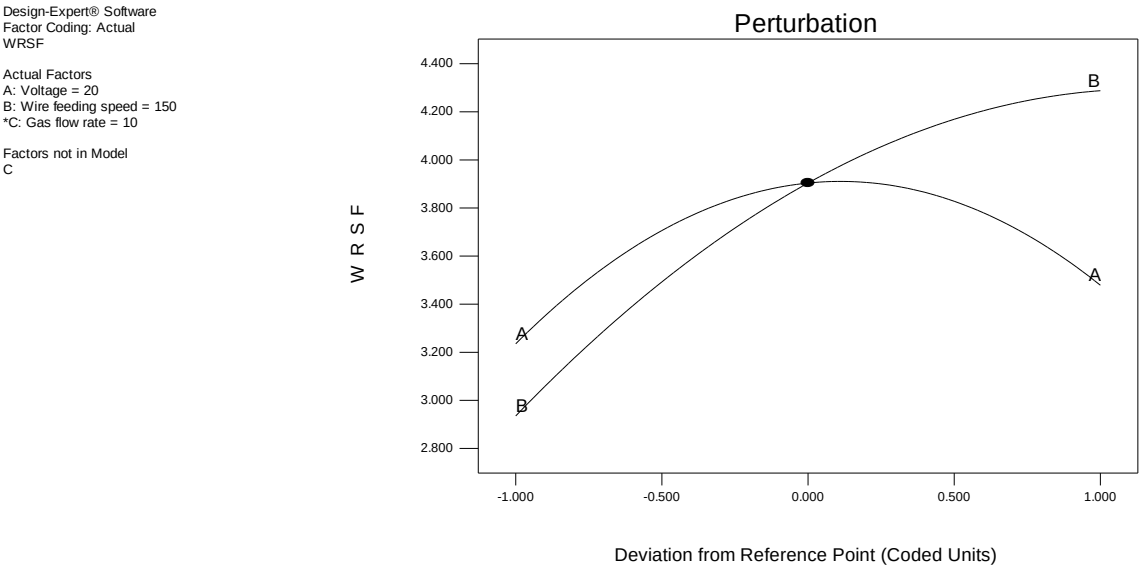


**Figure 12.** Perturbation of WRFF on wire feeding speed and gas flow rate.

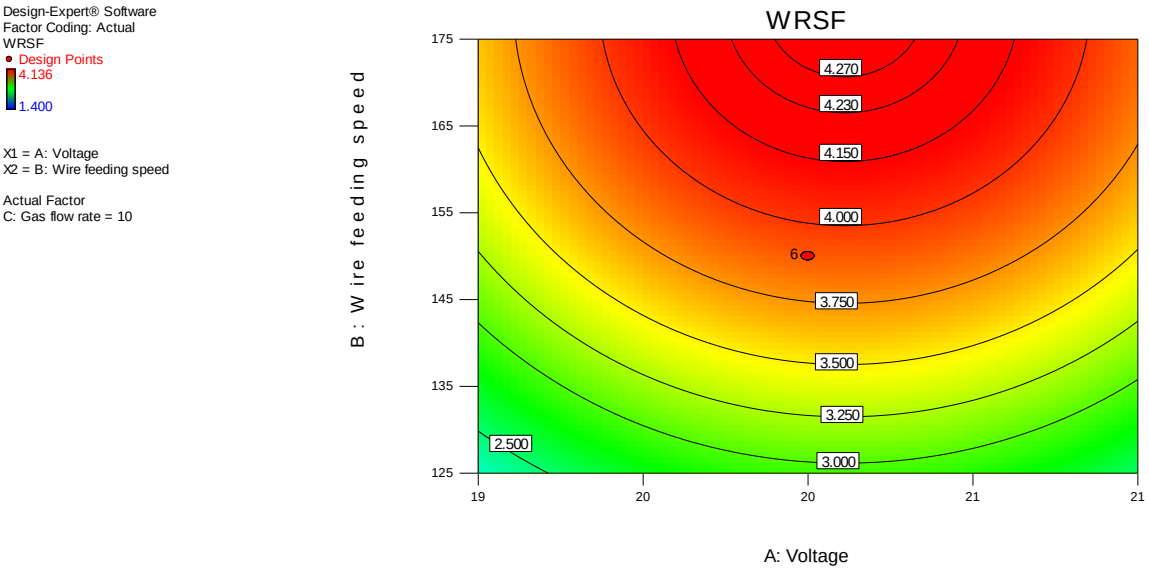


**Figure 13.** Contour graph of WRFF (or WRSF)welding velocity as a function of voltage and wire feeding speed gas flow rate 10 L/min.

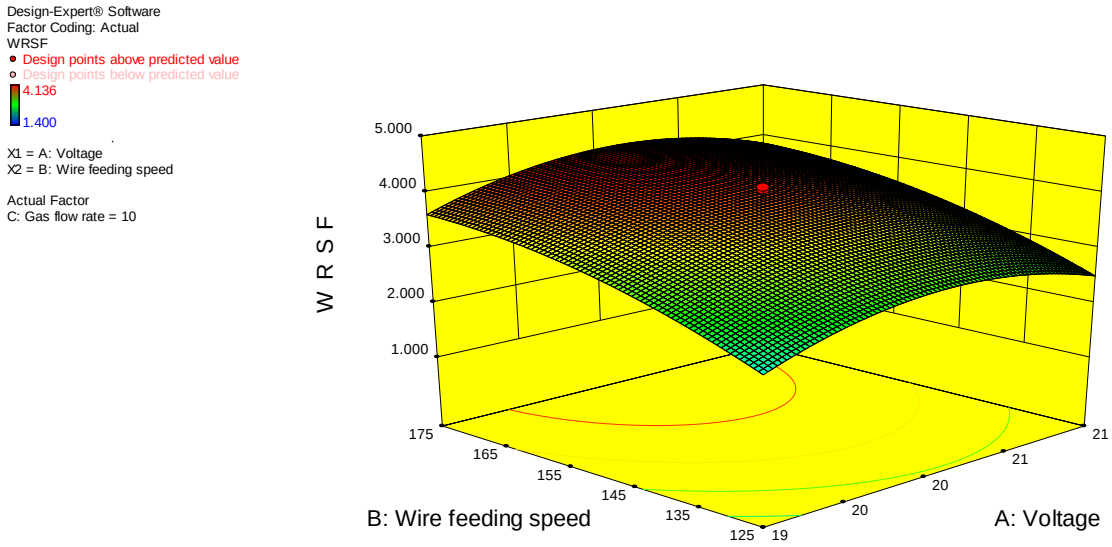


**Figure14.** 3D graph of WRFF as a function of voltage and wire feeding speed at gas flow rate 10 L/min.

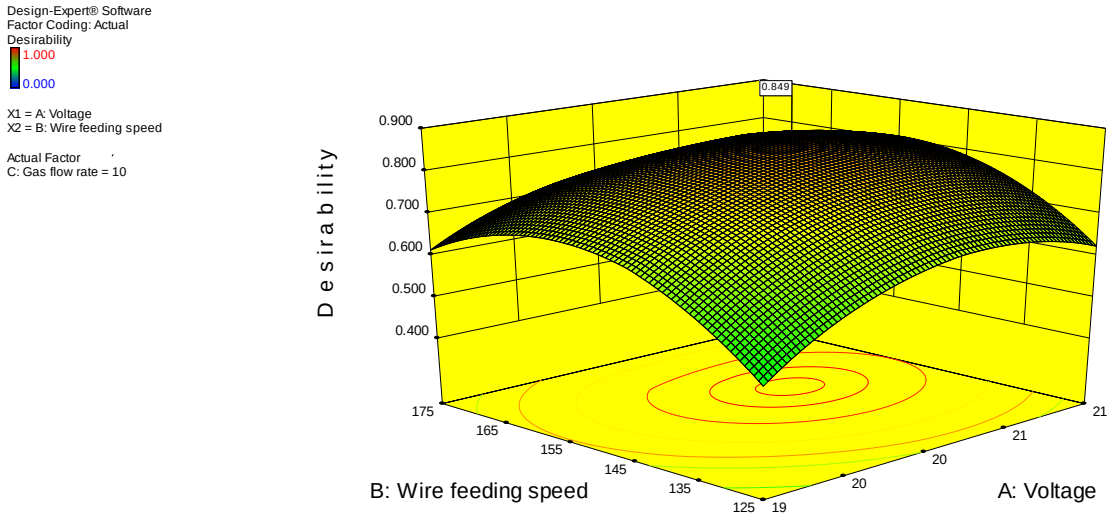


**Figure 15.** 3D graph for desirability as a function of voltage and wire feeding speed at gas flow rate 10 L/min.

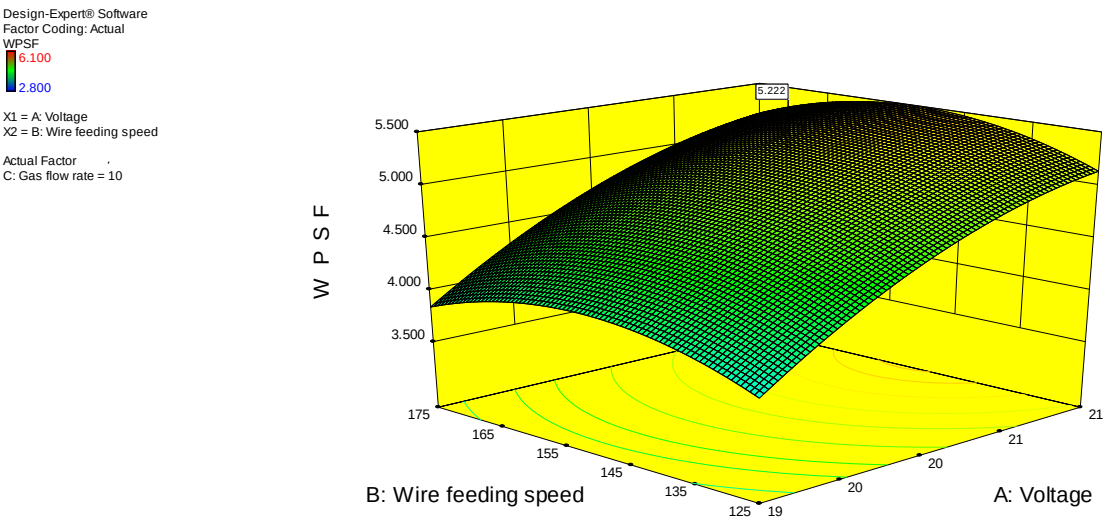


**Figure 16.** The optimum value for WPSF at 10 /min gas flow rate.

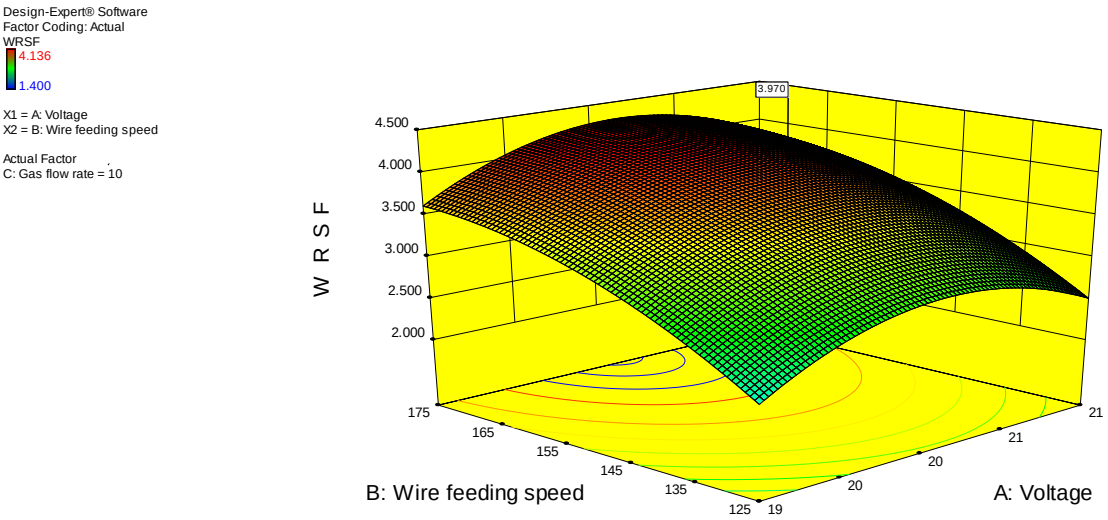


**Figure 17.** The optimum value for WRFF at 10 L/min gas flow rate.

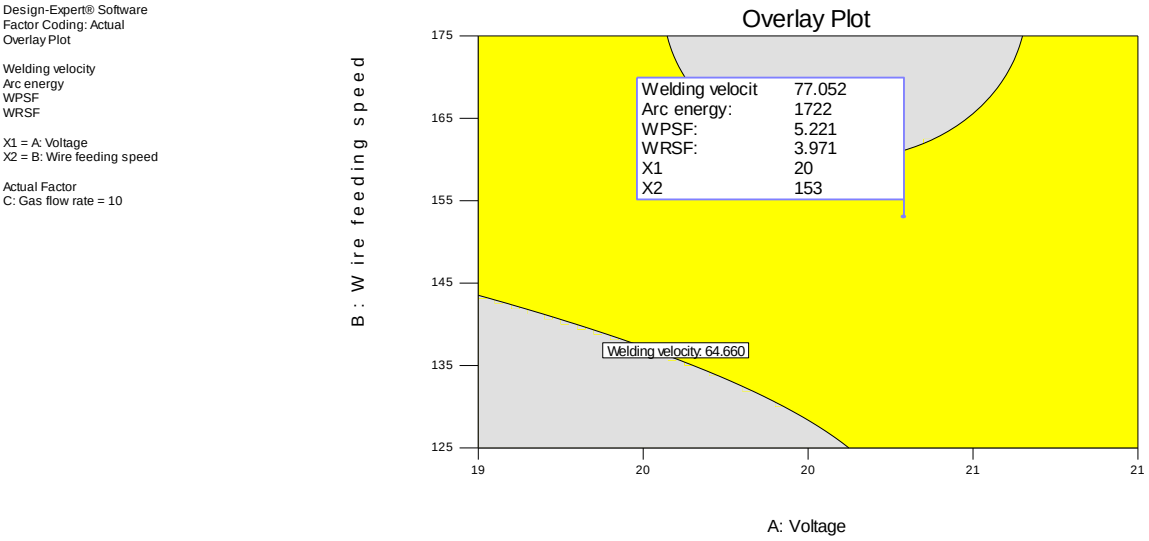


**Figure 18.** Overlay plot produced by numerical optimization showing the region of optimal welding variables at 10 L/min gas flow rate.